

LINNA: Likelihood Inference Neural Network Accelerator

Chun-Hao To ^{a,b,c,1} Eduardo Rozo^d Elisabeth Krause^{d,e} Hao-Yi Wu^f Risa H. Wechsler^{g,h,i} Andrés N. Salcedo^c

^aCenter for Cosmology and AstroParticle Physics (CCAPP), Ohio State University, Columbus, OH 43210, USA

^bDepartment of Physics, Ohio State University, Columbus, OH 43210, USA

^cDepartment of Astronomy, Ohio State University, Columbus, OH 43210, USA

^dDepartment of Physics, University of Arizona, Tucson, AZ 85721, USA

^eDepartment of Astronomy/Steward Observatory, University of Arizona, 933 North Cherry Avenue, Tucson, AZ 85721-0065, USA

^fDepartment of Physics, Boise State University, Boise, ID 83725, USA

^gDepartment of Physics, Stanford University, 382 Via Pueblo Mall, Stanford, CA 94305, USA

^hKavli Institute for Particle Astrophysics & Cosmology, P. O. Box 2450, Stanford University, Stanford, CA 94305, USA

ⁱSLAC National Accelerator Laboratory, Menlo Park, CA 94025, USA

E-mail: to.87@osu.edu, erozo@arizona.edu, krausee@arizona.edu,
hywu@boisestate.edu, rwechsler@stanford.edu, ansalcedo@arizona.edu

Abstract. Bayesian posterior inference of modern multi-probe cosmological analyses incurs massive computational costs. For instance, depending on the combinations of probes, a single posterior inference for the Dark Energy Survey (DES) data had a wall-clock time that ranged from 1 to 21 days using a state-of-the-art computing cluster with 100 cores. These computational costs have severe environmental impacts and the long wall-clock time slows scientific productivity. To address these difficulties, we introduce LINNA: the Likelihood Inference Neural Network Accelerator. Relative to the baseline DES analyses, LINNA reduces the computational cost associated with posterior inference by a factor of 8–50. If applied to the first-year cosmological analysis of Rubin Observatory’s Legacy Survey of Space and Time (LSST Y1), we conservatively estimate that LINNA will save more than US \$300,000 on energy costs, while simultaneously reducing CO₂ emission by 2,400 tons. To accomplish these reductions, LINNA automatically builds training data sets, creates neural network surrogate models, and produces a Markov chain that samples the posterior. We explicitly verify that LINNA accurately reproduces the first-year DES (DES Y1) cosmological constraints derived from a variety of different data vectors with our default code settings, without needing to retune the algorithm every time. Further, we find that LINNA is sufficient for enabling accurate and efficient sampling for LSST Y10 multi-probe analyses. We make LINNA publicly available at <https://github.com/chto/linna>, to enable others to perform fast and accurate posterior inference in contemporary cosmological analyses.

Keywords: Bayesian reasoning – cosmological parameters from LSS – machine learning – statistical sampling techniques

¹Corresponding author.

Contents

1	Introduction	1
2	Methods	2
2.1	LINNA design	2
2.2	Neural network	4
2.2.1	Neural network architecture	4
2.2.2	Loss function	5
2.2.3	Neural network optimization	6
3	Results and Discussion	7
3.1	6×2pt+N analysis	7
3.2	4×2pt+N analysis and 3×2pt analysis	9
3.3	Environmental Impact	10
4	Conclusions	12
A	Multidimensional comparison of two MCMC chains	15
B	Optimizations of the number of training data and run-time breakdowns	16
C	LSST Year 10 forecast	17

1 Introduction

Modern cosmological analyses typically employ a Bayesian framework, where posteriors are sampled using Markov Chain Monte Carlo (MCMC) techniques. Despite significant progress in the development of MCMC sampling algorithms [e.g. 1, 2], the computational requirements associated with performing these calculations can be significant. This is especially true for multi-probe analyses [3–7], which typically require the introduction of many tens of nuisance parameters to account for systematic effects presented in the data. As a specific example, the joint analysis of clusters, weak lensing, and galaxy clustering of [7] required 26 nuisance parameters. To achieve a well-sampled posterior, the chains in that analysis required at least five million likelihood evaluations, totaling $\sim 50k$ CPU hours. That is, a single run had a wall-clock time of *three weeks* using a state-of-the-art computing cluster with 100 cores.

The primary difficulty in this type of analysis is that the theory model used to evaluate the likelihood is computationally expensive. One way to bypass this limitation is to rely on fast surrogates of said model [e.g. 8–12]. However, the surrogates are typically built in pre-defined parameter spaces that are narrower than those used in most cosmological analyses. That is, the use of surrogates that are constructed *a priori* either limits the choice of priors that can be employed, or requires extrapolations of the surrogate outside the parameter regions over which the surrogate was calibrated.

To address these shortcomings, as well as to avoid having to build surrogates of theory models on a case-by-case basis, we present a new posterior inference tool: the Likelihood Inference Neural Network Accelerator (LINNA). LINNA is designed to enable fast and accurate posterior inference with arbitrary priors through the use of automatically built surrogates of the theory model. Given

the priors of the parameters, a theory model, the corresponding posterior function, and an efficient MCMC sampling algorithm, LINNA automatically generates training data, trains a neural network emulator of the model predictions, and samples the posterior using the provided MCMC sampling algorithm. The training data for the neural network emulator is generated in an iterative fashion designed to achieve accurate posteriors.

In this paper, we demonstrate that LINNA succeeds in accurately recovering the parameter posteriors derived from three different data vectors derived from the Dark Energy Survey [13] year 1 analyses (DES Y1):

1. 3×2pt, a joint analysis of galaxy clustering, galaxy–galaxy lensing, and cosmic shear [3].
2. 4×2pt+N, a joint analysis of cluster–galaxy cross correlations, cluster lensing, cluster clustering, and cluster abundances [7, 14].
3. 6×2pt+N, a joint analysis of data vectors in 3×2pt and 4×2pt+N. [7]

Further, we explicitly demonstrate that LINNA accurately reproduces the forecasted constraints for Rubin Observatory’s Legacy Survey of Space and Time (LSST) Year 10 data set (see appendix C for details).

This paper is organized as follows: In section 2, we describe the design of LINNA, the architecture of the neural network, the generation of training data, and the optimization of neural network parameters. In section 3, we demonstrate that LINNA can properly sample the posteriors of 6×2pt+N (section 3.1), 4×2pt+N (section 3.2), and 3×2pt (section 3.2). We further compare the performance of LINNA to a promising fast sampler BAYESFAST. The amount of reduction on CO₂ emission by using LINNA is estimated in section 3.3. A concluding remark is presented in section 4.

2 Methods

2.1 LINNA design

LINNA uses neural networks to create fast surrogates of computationally expensive theory models. This emulator can then be used in combination with efficient posterior sampling algorithms to quickly recover accurate approximations of the parameter posteriors. There are three main reasons why this approach is attractive:

1. Within the context of posterior estimation, the parameter space of interest has a well-defined boundary: the prior. This boundary makes it possible to generate a training set that spans the entire parameter space. This ensures that the LINNA emulator never extrapolates outside the domain over which it has been trained.
2. The neural network surrogate is differentiable, allowing the use of more efficient sampling algorithms, such as the Hamiltonian Monte Carlo (HMC). In practice, existing HMC codes are not parallelized, which incurs a significant penalty in the wall-clock time required to generate an MCMC chain relative to less efficient but fully parallelized sampling schemes.
3. Because the posteriors are sampled using standard techniques, we may readily use well-tested convergence tests of the resulting chains.

Despite these features, a significant problem remains. In high-dimensional parameter spaces, the volume of reasonably defined priors can greatly exceed the volume of the posteriors. Consequently,

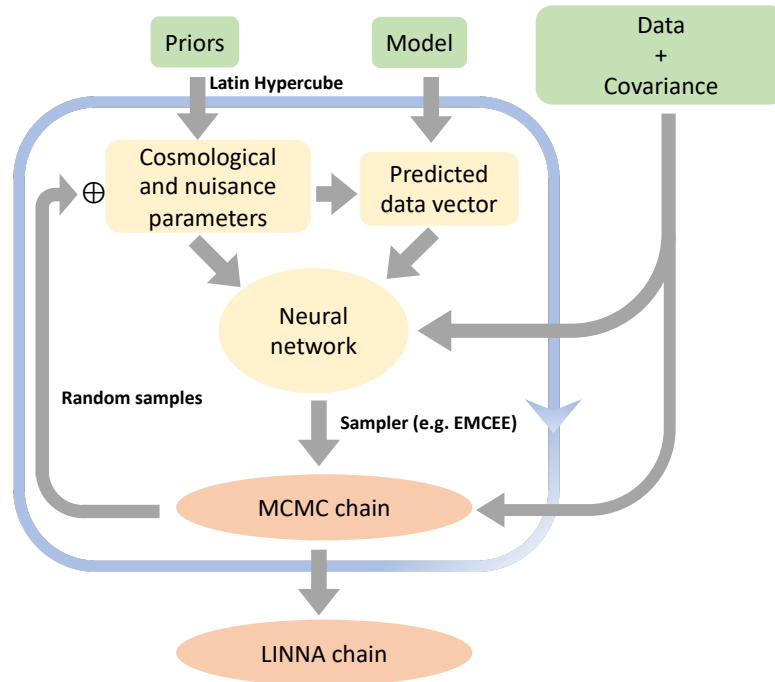


Figure 1. Outline of LINNA structure. Green blocks indicate inputs provided by users and orange blocks represent outputs of LINNA. Blocks within the blue rectangular are run iteratively. The symbol \oplus represents the procedure of expanding the training data by randomly sampling the MCMC chain from the previous iteration.

uniform sampling of the prior is extremely inefficient: it is likely that only a few training points fall within one- to three- sigma region of the posteriors, where high accuracy of the neural network surrogates is most desirable. We solve this problem using an iterative approach. In particular, a crude neural network is trained on a training set that uniformly samples the priors. This neural network is then fed into a posterior sampling tool to produce a MCMC chain, from which additional training data is generated. In this way, we construct a training set that covers the entire prior volume and is also capable of accurately reconstructing the parameter posteriors with comparatively little training data.

In the first few iterations, the neural network surrogates are rough at best, so their high-confidence regions can be offset from those of the true posterior. To overcome this problem, for the first few iterations of the algorithm, we enlarge the parameter posteriors using a temperature parameter T such that

$$\chi_T^2 = \chi_{\text{NN}}^2 / T^2, \quad (2.1)$$

where χ_{NN}^2 is the χ^2 value of the data calculated using neural network surrogates. We can think of this scaling as simply increasing all observational errors by a factor of T . The resulting broadening allows for the posteriors of the neural network surrogate model to be offset from the true posterior while still completely covering the same. In this way, when we generate new training data from the surrogate posterior we are able to improve the performance of the network over the true parameter posterior, even if the latter was offset from that of the approximate model. Initially, the temperature T should be set to a large value to ensure that the training data spans a wide enough parameter space. In the subsequent iterations, T can be gradually decreased due to the increasing accuracy of the neural network model over the region of interest. Empirically, we find that setting $T = 4$ and 2 for the first two iterations and $T = 1$ for all subsequent iterations leads to good posteriors.

We summarize the workflow for LINNA in figure 1. First, we use Latin Hypercube sampling of the prior volume space to generate an initial set of training points. At each training point, we use the provided theory model to evaluate the expectation value of the observable. The resulting training points and model expectations are used to train a neural network to arrive at our first surrogate model. This surrogate model in combination with the provided likelihood function, which is scaled by the appropriate temperature parameter, is fed to a standard sampling algorithm to arrive at MCMC samples of the posterior. The resulting chain is then randomly sampled to expand the number of points in the parameter space at which the neural network is trained. The procedure is iterated, decreasing the temperature from iteration to iteration as described above.

We run LINNA using the two publicly available posterior sampling code `EMCEE` [15] and `ZEUS` [2]. The convergence criteria are set based on the integrated autocorrelation time τ [16]. Specifically, let τ_i be the integrated autocorrelation time estimated using a chain of length i for each walker. A chain is considered converged if the following three criteria are met:

1. The autocorrelation time estimation is stable, i.e., $\tau_i/\tau_{i-100} - 1 < \eta$, where η is a user-specified parameter.
2. The number of steps per walker in units of the autocorrelation time is large, i.e., $i/\tau_i > \alpha$, where α is user-specified criterion.
3. The mean and error of each parameter estimated from the MCMC chain are stable. We first select the last $\beta \times \tau_i$ samples for each walker to remove the burn-in steps. We compute the estimated mean of each parameter (p) using the first and second half of the selected MCMC samples ($\mu_{1,p}$ and $\mu_{2,p}$ respectively). The error of each parameter is also estimated using the standard deviation of the first and second half of the MCMC samples ($\sigma_{1,p}$ and $\sigma_{2,p}$ respectively). The chain is converged if $\max_p(\|\mu_{1,p} - \mu_{2,p}\|/\sigma_{2,p}) < \delta_\mu$ and $\max_p(\|\sigma_{1,p}/\sigma_{2,p} - 1\|) < \delta_\sigma$.

The above criteria are checked for every 100 evaluation per walker. The parameters η , α , δ_μ , and δ_σ set the convergence criteria for the posterior sampling. We remove burn-in steps by keeping only the last $\beta \times \tau_i$ steps of each chain. Empirically, we have found the following settings provide accurate posteriors using 128 walkers:

- For `EMCEE`, the values of the parameters η , α , and β are set to $\eta = [0.03, 0.03, 0.02, 0.01]$, $\alpha = [5, 5, 10, 15]$, and $\beta = [2, 2, 5, 4]$, where [...] denotes the value for each iteration. δ_μ and δ_σ are set to 0.2 and 0.15 respectively for all iterations.
- For `ZEUS`, all parameters are kept the same, except for the value of α in the last iteration. The speed of `ZEUS` allows us to run a much longer chain with a modest increase of the overall run time. We therefore adopt $\alpha = 50$ in the last iteration.

2.2 Neural network

2.2.1 Neural network architecture

An artificial neural network (or simply neural network) is an interconnection of nodes that mimic the neural structures of the brain. The basic components of a neural network are nodes and connections between nodes. A node receives multiple inputs, calculates their weighted sums, adds an optional bias term, and passes the weighted sum through a non-linear function to produce the output. Connections between nodes specify the weights used in the weighted sum calculations. A neural network architecture specifies how nodes are connected, and it can drastically affect the performance of a neural network on a specific problem [e.g. 17]. One commonly used neural network architecture simply

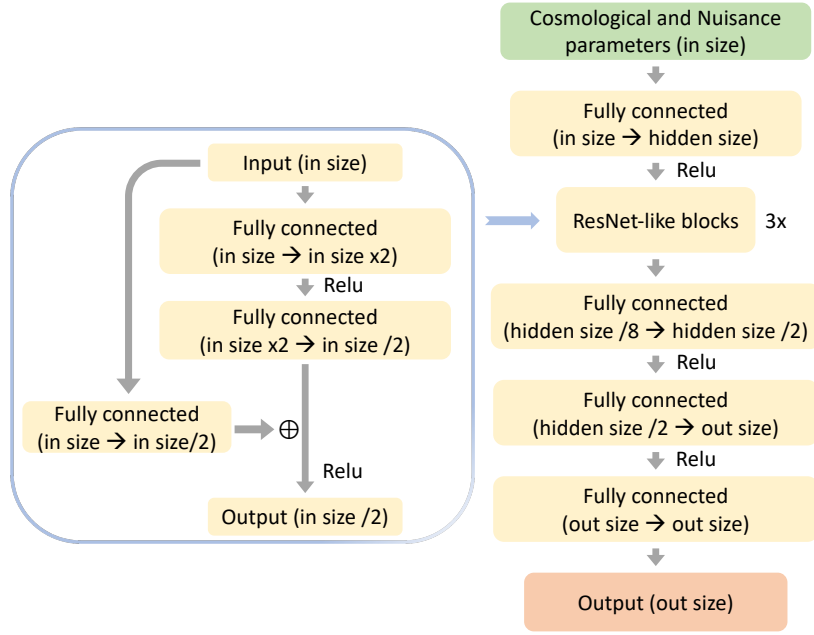


Figure 2. The architecture of the neural network in LINNA. Green blocks represent input of the network and orange blocks represent the output. Numbers in parentheses show the size of input and output vectors of each block. Hidden size is set to the minimum value of 32 times output vector size and 1000. Relu represents the Rectified Linear Unit, a widely used nonlinear function. The symbol \oplus denotes element-wise addition.

arranges nodes into multiple groups (often called layers) and connects all the nodes from one group to another. This network structure is often referred to as a multilayer perceptron and has been widely used in the cosmology community [e.g. 12, 18–20].

Despite their broad applicability, neural networks with multiple layers are difficult to train and their accuracy is not necessarily better than neural networks with fewer layers. This is known as the Degradation Problem: with increasing numbers of layers, the accuracy of a neural network gets saturated and can degrade [21]. This problem can be mitigated via introductions of “shortcut” connections [21], which provide connections that skip one or more layers. Inspired by [21], we modify the widely used multilayer perceptron architectures, which consists of multiple fully connected layers, by adding three shortcut connections for LINNA. The resulting neural network architecture is shown in figure 2.

2.2.2 Loss function

The loss function is judiciously chosen based on the task at hand, namely recovering accurate posteriors from the data. To that end, the loss function is motivated by two observations.

First, the accuracy requirement of the surrogate model is set by the noise of the data, i.e., noisy data do not require accurate models. Consequently, instead of using a uniformly weighted loss function, we weight the differences between the training data and the surrogate model by the inverse of the covariance matrix of the data.

Second, for the purposes of sampling posteriors, the surrogate model needs only to achieve high accuracy over high-likelihood regions. That is, whether a point in the parameter space has a posterior value that is 10^{-10} or 10^{-20} is irrelevant; we only need to know that this point is ruled out at high confidence. For this reason, we upweight the importance of those points in the parameter space that

are a good fit to the data by dividing their contribution to the loss function by the χ^2 of the model. Our loss function is therefore defined as

$$Loss = \left\langle \frac{(NN - M)^T C^{-1} (NN - M)}{(M - d)^T C^{-1} (M - d)} \right\rangle, \quad (2.2)$$

where NN denotes the output of the neural network, M represents the (actual) model prediction, C is the covariance matrix, d is the data vector, and $\langle \dots \rangle$ refers to the mean over training points.

2.2.3 Neural network optimization

The accuracy of the neural network increases as the training set expands, at the cost of increasing the computation expense of generating training data and training the neural network. We find that in each iteration of our algorithm, expanding the set of points used for training and validation by 10,000 and 500 respectively leads to a good compromise between accuracy and speed (see appendix B for details).

We also find that the performance improves if the training data are standardized before they are used to train the neural network. That is, the input of the neural network (i.e., the cosmological and nuisance parameters) is rescaled such that the entire training set has zero means and unit standard deviations. The model predictions are also rescaled judiciously. Specifically, let \vec{d}_α be the model prediction at the training point α , and d_α^i be the i^{th} element of the data vector \vec{d}_α . We rescale each training point via

$$d_\alpha^i \rightarrow \frac{d_\alpha^i}{\sigma^i} \quad (2.3)$$

where $(\sigma^i)^2$ is the i^{th} diagonal entry of the covariance matrix used to compute the likelihood function. We further define

$$\mu^i = \text{median}_\alpha(d_\alpha^i) \quad (2.4)$$

$$s^i = \text{MAD}_\alpha(d_\alpha^i), \quad (2.5)$$

where MAD refers to the median absolute deviation. Notice that the median values that define μ^i and s^i are over the set of training data (index α), and are computed for each individual data point (index i). With these quantities in hand, we further rescale the training data via

$$d_\alpha^i \rightarrow \frac{d_\alpha^i - \mu^i}{s^i}. \quad (2.6)$$

We find that rescaling by the median/MAD performs significantly better than rescaling by the mean and standard deviation, as the latter two are much more sensitive to a few outliers in the training data. The original data vector d^i can be recovered from the emulated data vector \vec{d}^i by applying the inverse transformation, i.e.

$$d^i = (\vec{d}^i s^i + \mu^i) \sigma^i. \quad (2.7)$$

During training, the training set is randomly shuffled and split into batches, each containing 500 points. The loss function is estimated using each batch of the training data and weights of the neural network are updated using the estimated loss function. We update the weights of the neural network using ADAMW [22], with an initial learning rate determined following methods described in [23] and an initial weight decay parameter of 10^{-4} .

The stop condition for the training of the neural network is set using the validation data. Specifically, after the network is updated using all batches of the training data, we evaluate the loss

function on the validation data. The learning rate is decreased by half when the minimum loss in the validation data is not updated after 450 steps. During the training, we use 200 steps to estimate the local derivative of the loss at a step. If the derivative is negative on the training set but positive on the validation set, the weight decay parameter is doubled to prevent over-fitting. The training process is automatically terminated when the minimum loss in the validation data is not updated after 500 steps.

The posterior is sampled using the trained neural network with the use of Intel Math Kernel Library for Deep Neural Networks ¹, which increases the evaluation speed by more than a thousand times relative to not using it.

3 Results and Discussion

We now test the performance of LINNA in a real-world scenario. Specifically, we compare the posterior estimated using LINNA to that estimated using `EMCEE` to sample the posterior function implemented in `COSMOLIKE` [24] (hereafter, the “brute force method”). Consequently, for the purpose of this comparison, the results presented here are obtained using `EMCEE` as the LINNA sampler and `COSMOLIKE` as the LINNA theory model. In practice, further improvements can be achieved using faster posterior sampling algorithms such as `ZEUS` (see figure 10 for details). The comparisons described in the main body of the paper are mostly visual (see figures 4, 5, and 6). A more rigorous comparison of the LINNA and “brute force method” chains can be found in Appendix A.

We perform all analyses using 128 CPU cores and 1 NVIDIA GeForce RTX 2080 Ti GPU on the Sherlock supercomputer². We consider three survey cosmology data vectors measured from first-year observations of DES (see a summary of these data vectors in figure 1 of [7]). Ranked by their computational cost, the three data sets are:

1. `6×2pt+N` [7]: a joint analysis of all data vectors in `3×2pt` and `4×2pt+N`.
2. `4×2pt+N` [7, 14]: a joint analysis of galaxy clustering, cluster–galaxy cross correlations, cluster clustering, cluster lensing, and cluster abundances.
3. `3×2pt` [3]: a joint analysis of galaxy clustering, galaxy–galaxy lensing, and cosmic shear.

In these analyses, we sample 32 (28, 26) cosmological and nuisance parameters for `6×2pt+N` (`4×2pt+N`, `3×2pt`) with the same priors presented in [7].

3.1 `6×2pt+N` analysis

figure 3 shows the 68% and 95% constraints on A_s and Ω_m using LINNA at each iteration. The blue points in the top row correspond to the 10,000 newly added training data points at each iteration, while the grey points represent the cumulative training data from previous iterations. In the first iteration, the training set is generated by uniformly sampling the prior volume using a Latin Hypercube. For the purposes of Latin Hypercube sampling, the boundaries of the parameters with Gaussian priors are set to $\pm n\sigma$ around their mean values, where n is a user-specified parameter. Throughout the analysis, we adopt $n = 3$ because the Gaussian priors are only applied to nuisance parameters, whose priors are conservatively chosen. We see that LINNA converges in just 3 iterations, though we advocate running an additional high-precision iteration to verify the convergence. For this reason, we adopt four iterations as our standard LINNA setting.

¹<https://github.com/rsdubtso/mkl-dnn>

²<https://www.sherlock.stanford.edu/>

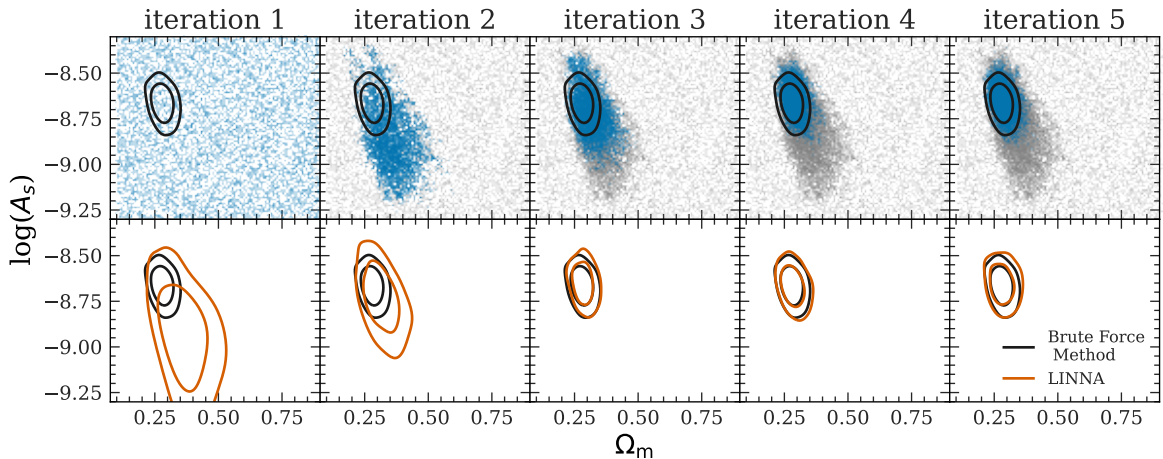


Figure 3. An illustration of the LINNA algorithm in the A_s – Ω_m parameter subspace, when applied to the $6 \times 2pt + N$ data set. Top row: distributions of training data. Training data from previous iterations are shown as grey dots while newly added training data are shown as blue dots. Black contours show the 68% and 95% contours of the targeted posteriors as evaluated using `EMCEE` to sample the posterior function implemented in `CosmoLike` (the brute force method). Bottom rows: comparison of LINNA posteriors (orange) to the target posterior (black) at each iteration. LINNA shows strong consistency with the brute force method after three iterations. We note that while we only show Ω_m and A_s in this plot, LINNA shows strong consistency with the brute force method after three iterations in all other cosmological and nuisance parameters as well.

figure 4 compares the final constraints obtained with LINNA (orange contours) to those derived using the brute force method (black contours). The comparison is restricted to the most important parameters in the analyses: Ω_m , A_s , two nonlinear intrinsic alignment parameters (A_{IA} , η_{IA}), and four richness–mass relation parameters ($\ln\lambda_0$, $A_{\ln\lambda}$, $B_{\ln\lambda}$, $\sigma_{\ln\lambda}$). We find excellent agreement between the two posteriors, with a shift in the mean parameter constraints of less than 0.2σ . The one-sigma errors on individual parameters all agree to better than 12%. A more detailed comparison of the means and errors between the two posteriors is shown in figure 7. Critically, LINNA ran ~ 10 hours, compared to ~ 3 weeks for the brute force method. A breakdown of total run time in each component of LINNA is further shown in table 1. As noted earlier, the run time can be further reduced by decreasing the number of training data and by replacing `EMCEE` with `ZEUS` in LINNA. Specifically, LINNA can reach similar performances on all constrained cosmological and nuisance parameters with the run time down to 5.5 hours.

We also compare our results to those obtained using `BAYESFAST` [1]³, another posterior inference acceleration code currently in development (green contours in figure 4). Similar to LINNA, `BAYESFAST` builds surrogate models by fitting quadratic polynomials to training data set in an iterative fashion. At each iteration, `BAYESFAST` samples the approximate posterior using the No U-Turn Hamiltonian Monte Carlo algorithm [25]. After the last iteration, it importance samples the chain by comparing the likelihood evaluated using the surrogate model and the likelihood evaluated using the full theory model. Using the same MCMC convergence criteria and hardware as LINNA, we find that `BAYESFAST` converges in 5.8 hours, a run time comparable to that of LINNA using `ZEUS` with 2000 training points. However, figure 4 demonstrates that the accuracy in the recovered posteriors of `BAYESFAST` is slightly worse than LINNA.

³<https://github.com/HerculesJack/bayesfast>

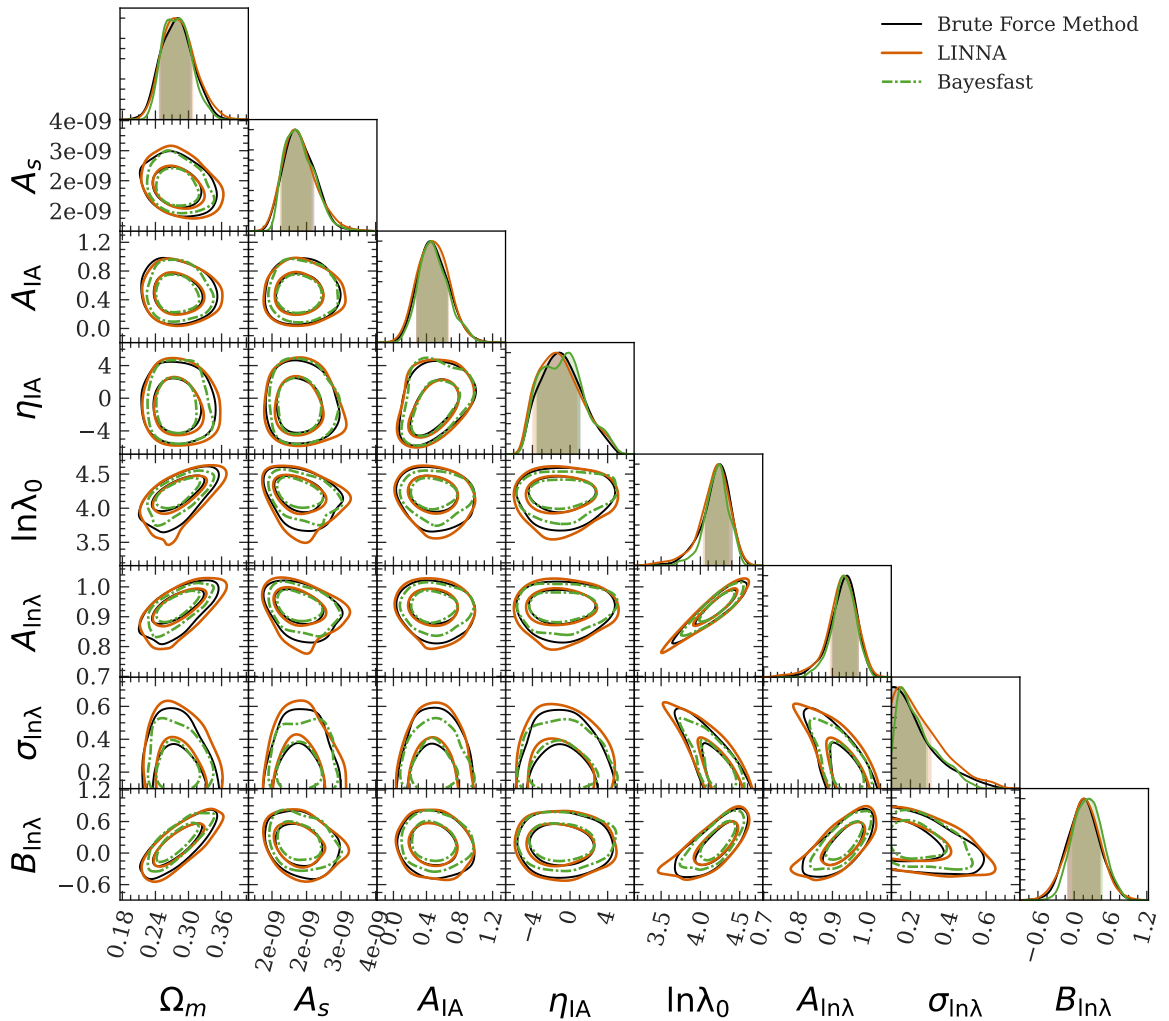


Figure 4. Constraints on important parameters when fitting to $6\times 2\text{pt}+N$ after marginalizing over additional 24 nuisance parameters. Black contours are obtained with the brute force method (EMCEE+CosmoLike), orange contours are obtained with LINNA, and green contours are obtained using BAYESFAST. Contours show 68% and 95% constraints.

3.2 $4\times 2\text{pt}+N$ analysis and $3\times 2\text{pt}$ analysis

figure 5 compares the posteriors derived for the $4\times 2\text{pt}+N$ data vector using LINNA (orange contours), the brute force method (EMCEE+CosmoLike, black contours) and BAYESFAST (green contours). As before, we restrict the figure to the most important parameters for the $4\times 2\text{pt}+N$ data vector. All samplers are run with exactly the same setting as for the $6\times 2\text{pt}+N$ analysis. The agreement between LINNA and the brute force method is remarkable and demonstrates that LINNA’s hyperparameters do not need to be retuned when running in subsets of the original data used to tune LINNA. This is not a trivial statement: BAYESFAST posteriors, which were only modestly biased for $6\times 2\text{pt}+N$ data set, are now much more strongly biased than before. figure 6 compares the posteriors derived for the $3\times 2\text{pt}$ data vector from LINNA (orange contours), the brute force method (EMCEE+CosmoLike, black contours), and BAYESFAST (green contours). Here, LINNA and BAYESFAST are both in excellent agreement with the brute force method.

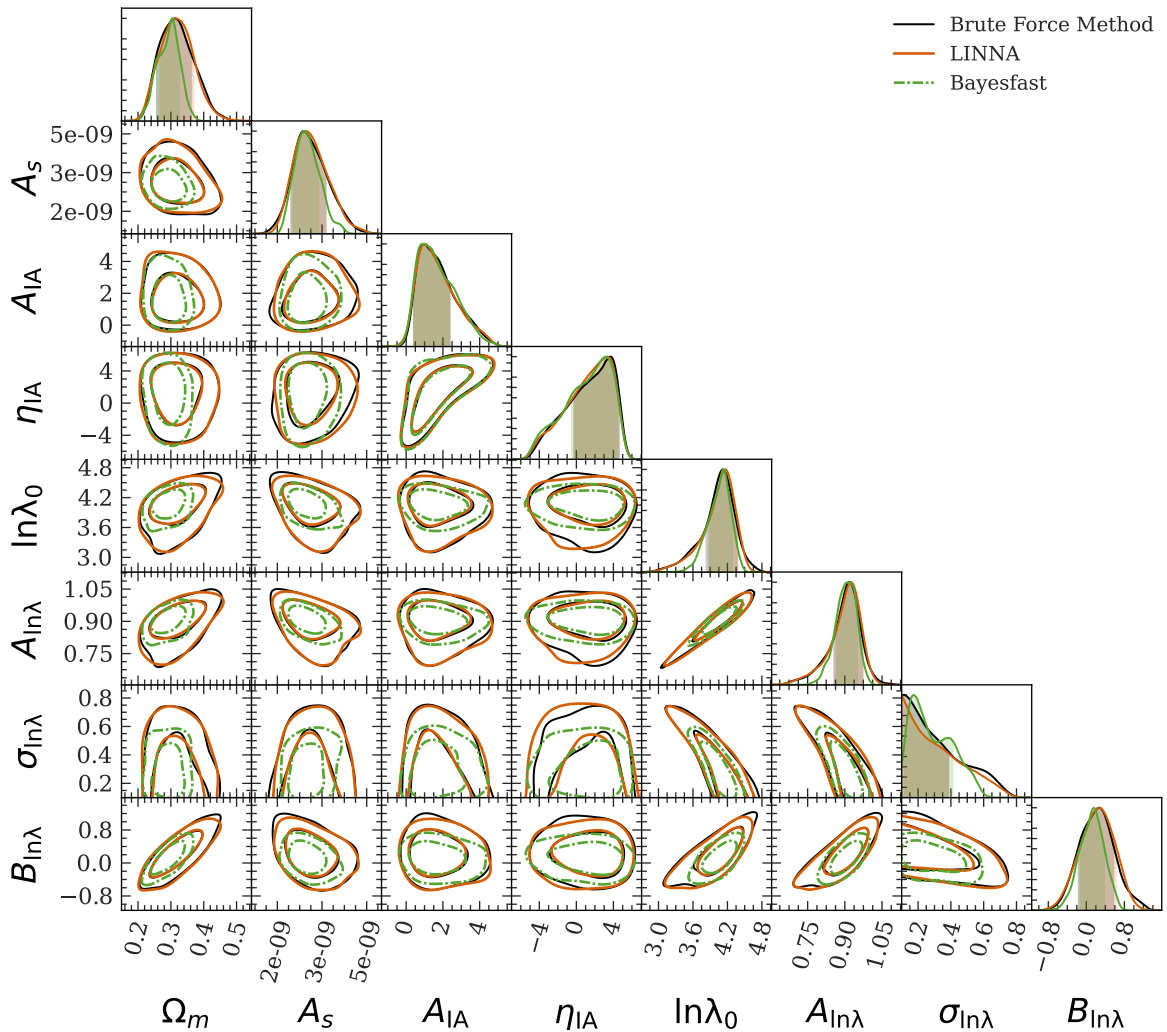


Figure 5. Similar to figure 4 but on $4 \times 2\text{pt} + \text{N}$ data vector.

As was the case for $6 \times 2\text{pt} + \text{N}$, using LINNA for these analyses leads to significant reductions in run time relative to the brute force method (EMCEE+CosmoLike). With the baseline setting, LINNA takes 11.5 (5.4) hours to sample the $4 \times 2\text{pt} + \text{N}$ ($3 \times 2\text{pt}$) posteriors, while the brute force method takes ~ 4 (1) days respectively. Again, LINNA can be further sped up while maintaining the same accuracy on all constrained parameters by decreasing the number of training data and by using faster samplers. With the same fast setting as used for $6 \times 2\text{pt} + \text{N}$, the run time of LINNA is 4.2 and 3.5 hours for $4 \times 2\text{pt} + \text{N}$ and $3 \times 2\text{pt}$ respectively.

3.3 Environmental Impact

Supercomputers have been recognized as a significant contributor to the CO_2 footprint of astronomical research [26–28]. To estimate the potential reductions of environmental impact by using LINNA, we first calculate the CO_2 emission savings associated with running one posterior inference analysis using LINNA versus the current standard approach (e.g. EMCEE+CosmoLike). [26] estimates that the energy consumption per CPU core is $\sim 53\text{W}$. The maximum electricity consumption of a NVIDIA GeForce RTX 2080 Ti GPU on the Sherlock supercomputer is 280W. Assuming the GPU is run with

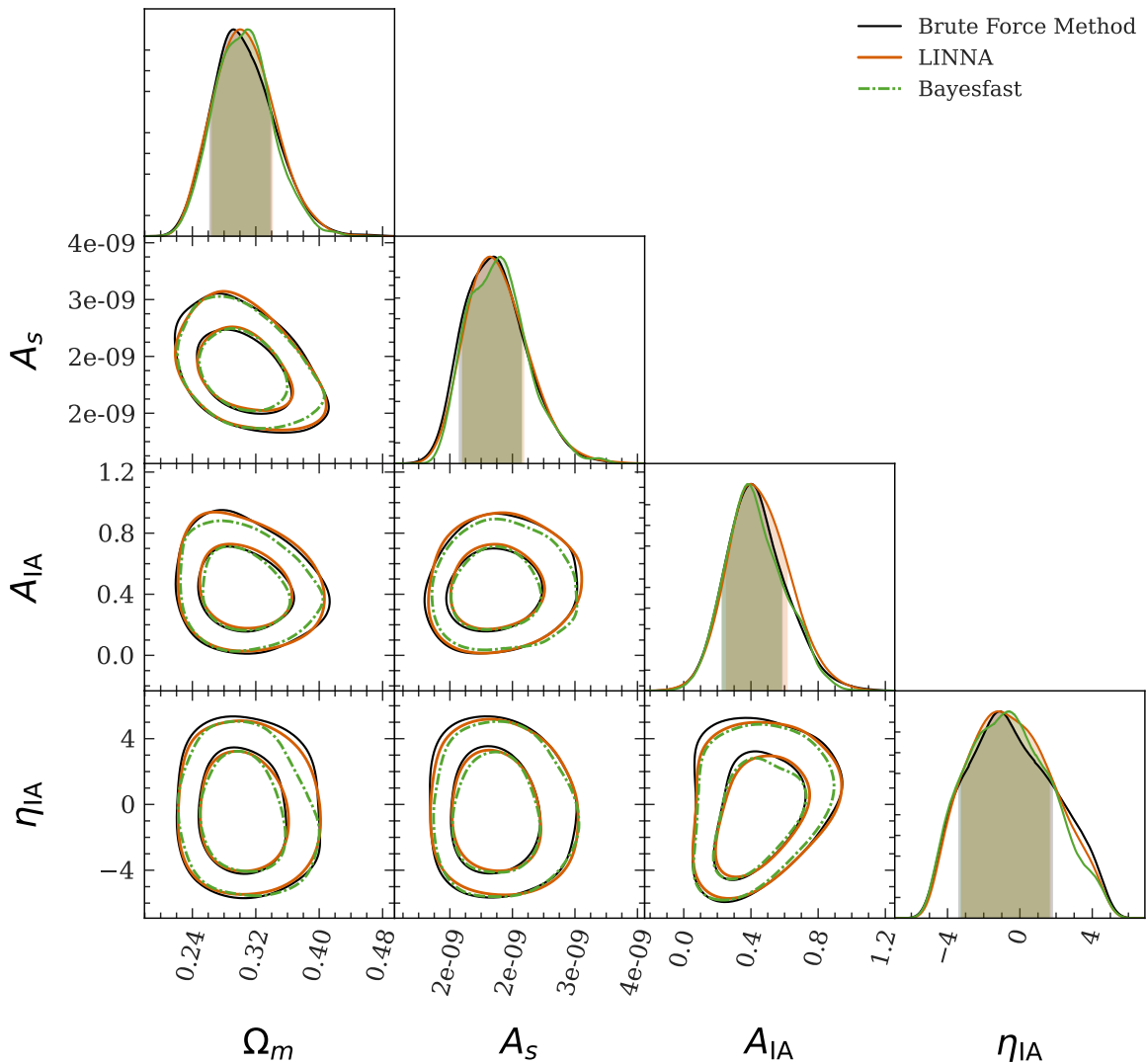


Figure 6. Similar to figure 4 but on 3×2 pt data vector.

the maximum power consumption during the entire analysis, we find that LINNA saves 12 billion Joule of electricity consumption per posterior inference analysis for 6×2 pt+N data vector. Assuming an average energy cost of US \$0.10 per kW-hour, as appropriate for the United States, this corresponds to US \$330 per posterior inference analysis. We translate this energy consumption to the amount of CO₂ emission using the EPA Carbon Offset Calculator ⁴ and find a reduction of 2.4 tons CO₂ emission per analysis.

Modern cosmology analyses typically require hundreds of posterior inference analyses to validate the analysis choices and modeling pipelines. For example, the DES collaboration performed over 900 posterior inference analyses to analyze the 3×2 pt data set measured from the first three years observations of DES. Therefore, we estimate that the publications of the cosmological constraints derived from first-year observations of Rubin observatory’s Legacy Survey of Space and Time (LSST Y1) will require $\sim 1,000$ posterior inference analyses. Assuming each posterior inference analysis of

⁴<https://www.epa.gov/energy/greenhouse-gas-equivalencies-calculator>

LSST Y1 has similar computational costs to those of the $6\times 2\text{pt}+\text{N}$ data set of DES Y1, we estimate that adopting LINNA for the LSST Y1 analysis will save upwards of US \$300,000 in energy costs, while simultaneously reducing the CO_2 footprint of the analysis by 2,400 tons of CO_2 . This is roughly equivalent to 2,400 transatlantic flights, or the yearly carbon footprint of 65 astronomers [29]. In practice, we expect the number of chains is likely to exceed our estimate, as we anticipate the data will be analyzed using many different theoretical approaches. In other words, relative to the DESY3 analyses, we have not scaled our estimates with collaboration size or model complexity in any way.

4 Conclusions

Posterior inference for modern survey cosmological analyses is computationally expensive. This is mostly due to the increasing complexity of the theory models needed to yield unbiased cosmological constraints from unprecedentedly precise measurements. This situation becomes more challenging when one considers multi-probe analyses, in which one analyzes different cosmological probes simultaneously to yield more robust and precise cosmological constraints. The complex data vector of multi-probe analyses requires one to sample more nuisance parameters that describe systematics of each individual probe, thereby severely increasing the dimensionality of the posteriors. These difficulties are especially pronounced in the case of cluster cosmology. Modeling of cluster-related two-point correlation functions requires marginalization over observable–mass relation and cluster-related systematics, such as selection biases [e.g. 14], cluster mis-centering [e.g. 30], and correlation coefficients between different cluster mass–observable connections [e.g. 31]. These additional modeling complexities significantly increase the computational cost of posterior inference. For instance, the run time for the $3\times 2\text{pt}$ analysis of the first-year data from the Dark Energy Survey [3] was ~ 1 day. With the same hardware, the corresponding $6\times 2\text{pt}+\text{N}$ analysis [7] took ~ 3 weeks.

In this work, we expedite the posterior inference by constructing a surrogate of expensive cosmological models using a deep neural network (see figure 2). We design an iterative process to build a training data set that both spans the entire prior volume and reasonably samples the posterior with a limited amount of total training data (summarized in figure 1). The trained surrogate model can be combined with standard posterior sampling tools to perform accurate Bayesian posterior inference analyses. We test the developed posterior inference accelerator LINNA on data vectors measured from the Dark Energy Survey first-year observations. In particular, we consider three data vectors: $3\times 2\text{pt}$ (a joint analysis of galaxy clustering, galaxy–galaxy lensing, and cosmic shear), $4\times 2\text{pt}+\text{N}$ (a joint analysis of cluster–galaxy cross correlations, cluster lensing, cluster clustering, and cluster abundances), and $6\times 2\text{pt}+\text{N}$ (a joint analysis of data vectors in $3\times 2\text{pt}$ and $4\times 2\text{pt}+\text{N}$). The results of our tests can be summarized as follows:

1. In all data vectors, the posteriors obtained from LINNA agree with those from the brute force method that uses `EMCEE` to sample the posterior implemented in `COSMOLIKE`. The hyperparameters of LINNA are fine-tuned for $6\times 2\text{pt}+\text{N}$, but stay the same for $4\times 2\text{pt}+\text{N}$ and $3\times 2\text{pt}$.
2. In the $6\times 2\text{pt}+\text{N}$ ($4\times 2\text{pt}+\text{N}$, $3\times 2\text{pt}$) analysis, the brute force method took ~ 3 weeks (~ 4 days, ~ 1 day) to sample the posterior using 128 CPUs while LINNA took 10.1 (11.5, 5.4) hours using 128 CPUs and 1 NVIDIA GeForce RTX 2080 Ti GPU. With the same performance on all constrained parameters, the run time of LINNA can be further reduced to 5.5 (4.2, 3.5) hours by reducing the number of training data and adopting `ZEUS` as the posterior sampler.
3. The reduced computational demands lead to a reduction of 12 billion Joules of electricity consumption per posterior inference analysis. We estimate that using LINNA for the LSST Y1

cosmological analysis will save \$300,000 in energy costs, while simultaneously reducing CO₂ emission by 2,400 tons, equivalent to the annual carbon footprint of ~ 65 astronomers.

While we have demonstrated the performance of LINNA using DES Y1 data set, we have also explicitly verified that LINNA accurately reproduces the forecasted constraints for LSST Y10 for the 3×2pt and 6×2pt+N data sets (see appendix C for details). Further, although the run times measured in this paper are based on COSMOLIKE and EMCEE, LINNA allows users to replace these components with other modeling codes and different samplers such as ZEUS [2] or MULTINEST [32] to further speed up the analysis. We make the LINNA package publicly available at <https://github.com/ghto/linna>, in the hope that it will prove useful for ongoing and future astronomical and cosmological analyses.

For discussions on an independently developed likelihood acceleration tool for LSST Year 1 3×2pt analyses, we refer the reader to [33].

Acknowledgements

CHT thanks Wei-Lin Chiang for helpful discussions on GPUs and neural networks and David Weinberg for insightful discussions. This work received support from the United States Department of Energy, Office of High Energy Physics under Award Number DE-SC-0011726 and under contract number DE-AC02-76SF00515 to SLAC National Accelerator Laboratory. ER is supported by DOE grant DE-SC0009913, NSF grant 2009401, and a Cottrell Scholar award. HYW is supported by DOE Grant DE-SC0021916 and NASA grant 15-WFIRST15-0008.

We acknowledge the use of GetDist [34], Pytorch [35], Matplotlib [36], and NumPy [37] for the analyses. Some of the computing for this project was performed on the Sherlock cluster at Stanford. We would like to thank Stanford University, the Kavli Institute for Particle Astrophysics and Cosmology, and the Stanford Research Computing Center for providing computational resources and support that contributed to these research results.

References

- [1] H. Jia and U. Seljak, *BayesFast: A Fast and Scalable Method for Cosmological Bayesian Inference*, in *prep.* (2022).
- [2] M. Karamanis, F. Beutler and J. A. Peacock, *zeus: A python implementation of ensemble slice sampling for efficient bayesian parameter inference*, *arXiv preprint arXiv:2105.03468* (2021).
- [3] T. M. C. Abbott, F. B. Abdalla, A. Alarcon, J. Aleksić, S. Allam, S. Allen et al., *Dark Energy Survey year 1 results: Cosmological constraints from galaxy clustering and weak lensing*, *Phys. Rev. D* **98** (Aug., 2018) 043526, [[arXiv:1708.01530](https://arxiv.org/abs/1708.01530)].
- [4] E. van Uitert, B. Joachimi, S. Joudaki, A. Amon, C. Heymans, F. Köhlinger et al., *KiDS+GAMA: cosmology constraints from a joint analysis of cosmic shear, galaxy-galaxy lensing, and angular clustering*, *MNRAS* **476** (June, 2018) 4662–4689, [[arXiv:1706.05004](https://arxiv.org/abs/1706.05004)].
- [5] S. Joudaki, C. Blake, A. Johnson, A. Amon, M. Asgari, A. Choi et al., *KiDS-450 + 2dFLenS: Cosmological parameter constraints from weak gravitational lensing tomography and overlapping redshift-space galaxy clustering*, *MNRAS* **474** (Mar., 2018) 4894–4924, [[arXiv:1707.06627](https://arxiv.org/abs/1707.06627)].
- [6] DES Collaboration, T. M. C. Abbott, M. Aguena, A. Alarcon, S. Allam, O. Alves et al., *Dark Energy Survey Year 3 Results: Cosmological Constraints from Galaxy Clustering and Weak Lensing*, *arXiv e-prints* (May, 2021) arXiv:2105.13549, [[arXiv:2105.13549](https://arxiv.org/abs/2105.13549)].
- [7] C. To, E. Krause, E. Rozo, H. Wu, D. Gruen, R. H. Wechsler et al., *Dark Energy Survey Year 1 Results: Cosmological Constraints from Cluster Abundances, Weak Lensing, and Galaxy Correlations*, *Phys. Rev. Lett.* **126** (Apr., 2021) 141301, [[arXiv:2010.01138](https://arxiv.org/abs/2010.01138)].

- [8] T. Auld, M. Bridges and M. P. Hobson, *COSMONET: fast cosmological parameter estimation in non-flat models using neural networks*, *MNRAS* **387** (July, 2008) 1575–1582, [[astro-ph/0703445](#)].
- [9] S. Agarwal, F. B. Abdalla, H. A. Feldman, O. Lahav and S. A. Thomas, *PkANN - II. A non-linear matter power spectrum interpolator developed using artificial neural networks*, *MNRAS* **439** (Apr., 2014) 2102–2121, [[arXiv:1312.2101](#)].
- [10] M. Pellejero-Ibañez, R. E. Angulo, G. Aricó, M. Zennaro, S. Contreras and J. Stücker, *Cosmological parameter estimation via iterative emulation of likelihoods*, *MNRAS* **499** (Dec., 2020) 5257–5268, [[arXiv:1912.08806](#)].
- [11] A. Spurio Mancini, D. Piras, J. Alsing, B. Joachimi and M. P. Hobson, *COSMOPOWER: Emulating cosmological power spectra for accelerated Bayesian inference from next-generation surveys*, *MNRAS* (Jan., 2022).
- [12] J. DeRose, S.-F. Chen, M. White and N. Kokron, *Neural Network Acceleration of Large-scale Structure Theory Calculations*, *arXiv e-prints* (Dec., 2021) arXiv:2112.05889, [[arXiv:2112.05889](#)].
- [13] A. Drlica-Wagner, I. Sevilla-Noarbe, E. S. Rykoff, R. A. Gruendl, B. Yanny, D. L. Tucker et al., *Dark Energy Survey Year 1 Results: The Photometric Data Set for Cosmology*, *ApJS* **235** (Apr., 2018) 33, [[arXiv:1708.01531](#)].
- [14] C.-H. To, E. Krause, E. Rozo, H.-Y. Wu, D. Gruen, J. DeRose et al., *Combination of cluster number counts and two-point correlations: validation on mock Dark Energy Survey*, *MNRAS* **502** (Apr., 2021) 4093–4111, [[arXiv:2008.10757](#)].
- [15] D. Foreman-Mackey, D. W. Hogg, D. Lang and J. Goodman, *emcee: The MCMC Hammer*, *PASP* **125** (Mar., 2013) 306, [[arXiv:1202.3665](#)].
- [16] J. Goodman and J. Weare, *Ensemble samplers with affine invariance*, *Communications in Applied Mathematics and Computational Science* **5** (Jan., 2010) 65–80.
- [17] A. Canziani, A. Paszke and E. Culurciello, *An analysis of deep neural network models for practical applications*, *CoRR abs/1605.07678* (2016) [[arXiv:1605.07678](#)].
- [18] T. Auld, M. Bridges, M. P. Hobson and S. F. Gull, *Fast cosmological parameter estimation using neural networks*, *MNRAS* **376** (Mar., 2007) L11–L15, [[astro-ph/0608174](#)].
- [19] S. Agarwal, F. B. Abdalla, H. A. Feldman, O. Lahav and S. A. Thomas, *PkANN - I. Non-linear matter power spectrum interpolation through artificial neural networks*, *MNRAS* **424** (Aug., 2012) 1409–1418, [[arXiv:1203.1695](#)].
- [20] C. Modi, Y. Feng and U. Seljak, *Cosmological reconstruction from galaxy light: neural network based light-matter connection*, *J. Cosmology Astropart. Phys.* **2018** (Oct., 2018) 028, [[arXiv:1805.02247](#)].
- [21] K. He, X. Zhang, S. Ren and J. Sun, *Deep Residual Learning for Image Recognition*, *arXiv e-prints* (Dec., 2015) arXiv:1512.03385, [[arXiv:1512.03385](#)].
- [22] Z. Xie, I. Sato and M. Sugiyama, *Understanding and Scheduling Weight Decay*, *arXiv e-prints* (Nov., 2020) arXiv:2011.11152, [[arXiv:2011.11152](#)].
- [23] L. N. Smith, *Cyclical learning rates for training neural networks*, in *2017 IEEE winter conference on applications of computer vision (WACV)*, pp. 464–472, IEEE, 2017.
- [24] E. Krause and T. Eifler, *cosmolike - cosmological likelihood analyses for photometric galaxy surveys*, *MNRAS* **470** (Sept., 2017) 2100–2112, [[arXiv:1601.05779](#)].
- [25] M. D. Homan and A. Gelman, *The no-u-turn sampler: Adaptively setting path lengths in hamiltonian monte carlo*, *J. Mach. Learn. Res.* **15** (jan, 2014) 1593–1623.
- [26] A. R. H. Stevens, S. Bellstedt, P. J. Elahi and M. T. Murphy, *The imperative to reduce carbon emissions in astronomy*, *Nature Astronomy* **4** (Sept., 2020) 843–851, [[arXiv:1912.05834](#)].
- [27] L. Burtscher, H. Dalglish, D. Barret, T. Beuchert, A. Borkar, F. Cantalloube et al., *Forging a sustainable future for astronomy*, *Nature Astronomy* **5** (Sept., 2021) 857–860.

- [28] F. van der Tak, L. Burtscher, S. Portegies Zwart, B. Tabone, G. Nelemans, S. Bloemen et al., *The carbon footprint of astronomy research in the Netherlands*, *Nature Astronomy* **5** (Dec., 2021) 1195–1198.
- [29] J. Knödlseeder, S. Brau-Nogué, M. Coriat, P. Garnier, A. Hughes, P. Martin et al., *Estimate of the carbon footprint of astronomical research infrastructures*, *arXiv e-prints* (Jan., 2022) arXiv:2201.08748, [[arXiv:2201.08748](#)].
- [30] T. McClintock, T. N. Varga, D. Gruen, E. Rozo, E. S. Rykoff, T. Shin et al., *Dark energy survey year 1 results: weak lensing mass calibration of redmapper galaxy clusters*, *MNRAS* **482** (Jan., 2019) 1352–1378, [[arXiv:1805.00039](#)].
- [31] S. Bocquet, J. P. Dietrich, T. Schrabback, L. E. Bleem, M. Klein, S. W. Allen et al., *Cluster Cosmology Constraints from the 2500 deg² SPT-SZ Survey: Inclusion of Weak Gravitational Lensing Data from Magellan and the Hubble Space Telescope*, *ApJ* **878** (June, 2019) 55, [[arXiv:1812.01679](#)].
- [32] F. Feroz, M. P. Hobson and M. Bridges, *MULTINEST: an efficient and robust Bayesian inference tool for cosmology and particle physics*, *MNRAS* **398** (Oct., 2009) 1601–1614, [[arXiv:0809.3437](#)].
- [33] S. S. Boruah, T. Eifler and V. Miranda, *Accelerating cosmological inference with Gaussian processes and neural networks*, *in prep.* (2022).
- [34] A. Lewis, *GetDist: a Python package for analysing Monte Carlo samples*, [arXiv:1910.13970](#).
- [35] A. Paszke, S. Gross, F. Massa, A. Lerer, J. Bradbury, G. Chanan et al., *Pytorch: An imperative style, high-performance deep learning library*, *Advances in neural information processing systems* **32** (2019) 8026–8037.
- [36] J. D. Hunter, *Matplotlib: A 2d graphics environment*, *Computing in Science & Engineering* **9** (2007), no. 3 90–95.
- [37] S. van der Walt, S. C. Colbert and G. Varoquaux, *The numpy array: A structure for efficient numerical computation*, *Computing in Science Engineering* **13** (March, 2011) 22–30.
- [38] The LSST Dark Energy Science Collaboration, R. Mandelbaum, T. Eifler, R. Hložek, T. Collett, E. Gawiser et al., *The LSST Dark Energy Science Collaboration (DESC) Science Requirements Document*, *arXiv e-prints* (Sept., 2018) arXiv:1809.01669, [[arXiv:1809.01669](#)].

A Multidimensional comparison of two MCMC chains

We wish to compare LINNA chains to those obtained using the brute force method. To do so, we compare the means and errors for each of the parameters in the model, as shown in figure 7. In the top row of figure 7, we show the difference in the mean between LINNA and the brute force method for each model parameter, in units of the standard deviation of the same (as evaluated using the brute force method). We find that the difference between the two means is always less than 0.2σ , with the median difference being 0.2σ . The figure also compares the EMCEE chains from the brute force method to those generated using MULTINEST. Notice the LINNA posteriors are in better agreement with the brute force method than those estimated using MULTINEST.

We further compare the uncertainty estimations from LINNA and those from the brute force method in the bottom row of figure 7. To make this comparison, we compute the parameter covariance matrix using chains from LINNA and chains from the brute force method. We rotate the covariance matrix estimated using the LINNA chain to the eigen-space of the covariance matrix estimated using the chain from the brute force method (reference covariance matrix hereafter). If the two covariance matrices are consistent, the rotated covariance matrix will be mostly diagonal with the diagonal value being identical to the eigen-value of the reference covariance matrix. In the bottom two panels of figure 7, we show that the rotated covariance matrix is mostly diagonal and the diagonal value is nearly

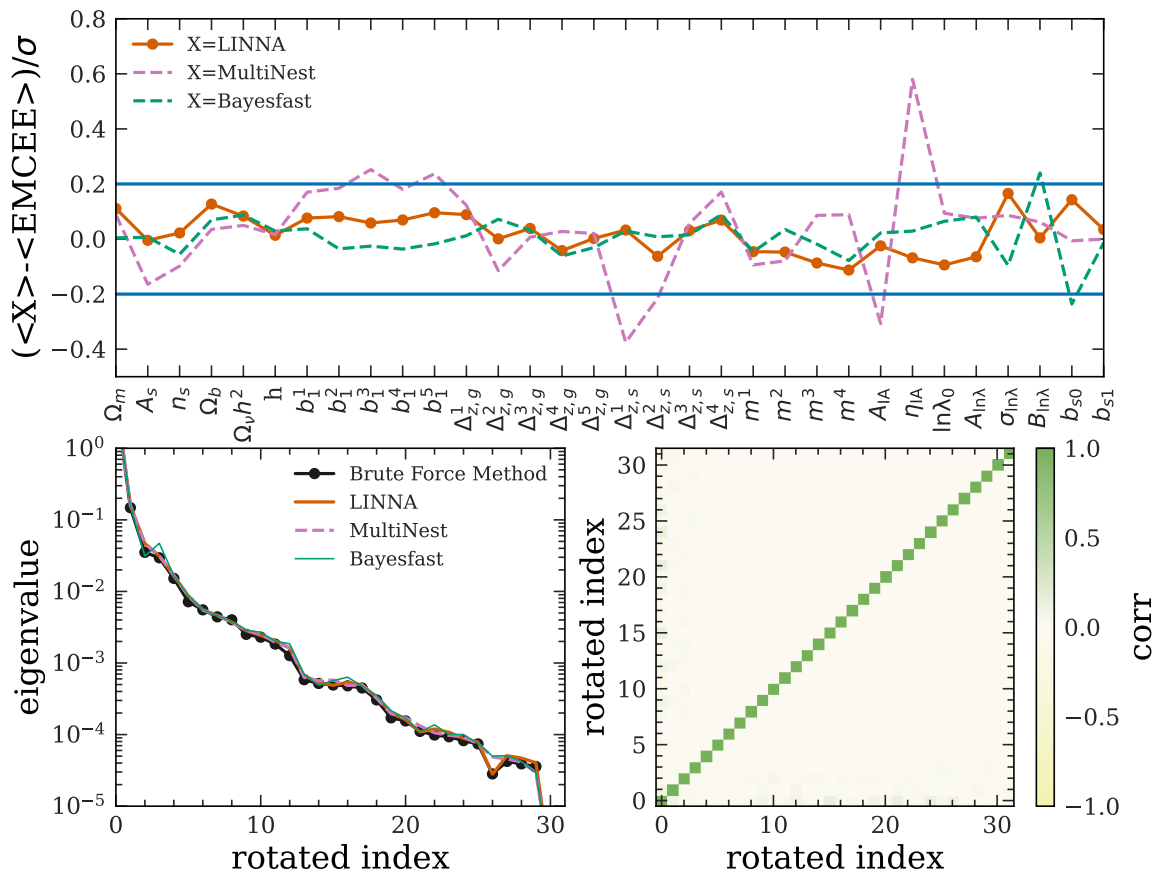


Figure 7. A comparison of multidimensional posteriors obtained with LINNA and with EMCEE from the $6 \times 2pt + N$ data vector. Top: a comparison of parameter means obtained with different samplers to 1σ uncertainties using EMCEE chains. Bottom left: a comparison of eigen-value of parameter covariance matrix estimated using EMCEE chains (black) and diagonal value of parameter covariance matrix estimated using LINNA (BAYESFAST) chains after they are rotated to the eigen-space of former (orange (green)). Bottom right: the correlation matrix of parameters estimated using LINNA chains after they are rotated to the eigen-space of parameter covariance matrix estimated using EMCEE chains.

identical to the eigen-value of the reference covariance matrix. Similar comparisons for $4 \times 2pt + N$ and $3 \times 2pt$ data vectors are shown in figure 8 and 9.

B Optimizations of the number of training data and run-time breakdowns

In figure 10, we compare the performance of LINNA with different numbers of training data points added in each iteration. We find that as long as the number of training data points added in each iteration is more than 2000, LINNA leads to less than 0.2σ shifts in all parameters that are meaningfully constrained by the data. With 10000 training data points added in each iteration, *all* parameters are shifted by less than 0.2σ when compared to the brute force method. We thus adopt adding 10000 training data points in each iteration as the default option for LINNA, but note that 2000 training data points could lead to a reasonable performance in all constrained parameters. In table 1, we show the breakdown of the total run time of LINNA with 10000 and 2000 training data points added in each iteration respectively. The total run time reduces from 10.1 hours to 6.89 hours when reducing the

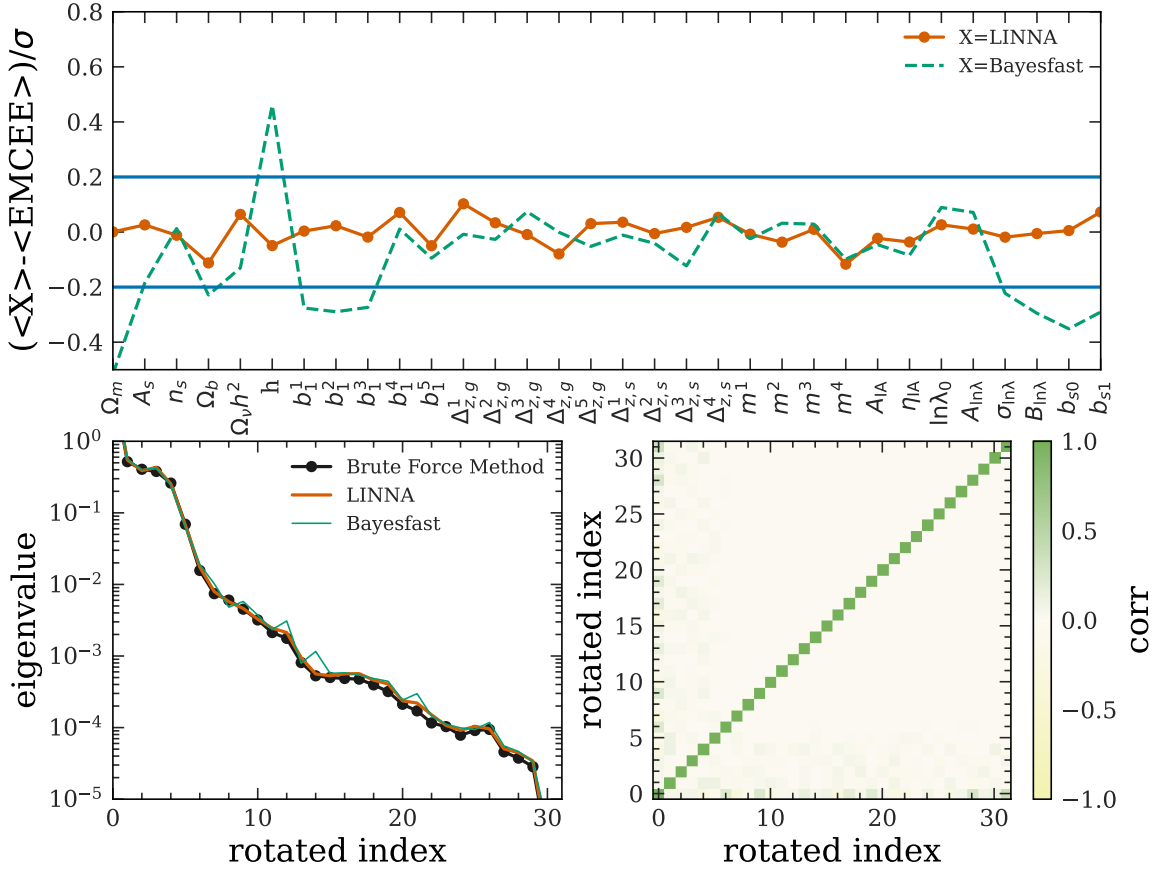


Figure 8. Similar to figure 7 but on the $4 \times 2pt + N$ data vector.

number of training data points from 10000 to 2000. We further note that in the case of 2000 training data points, the LINNA run time is dominated by the MCMC sampling. One could further speed up LINNA using faster samplers such as ZEUS. We find that using ZEUS reduces the run time for the 2000 training data point case to 5.52 hours while maintaining the same performance.

C LSST Year 10 forecast

We evaluate the expected performance of LINNA on ten-year LSST (LSST Y10) data using simulated data vectors. We construct the data vector using CosmoLike, using parameters described in [38]. For details, we refer the reader to To, Krause et al. in prep. Here, we provide a short description. The lens galaxy samples are split into 10 equally spaced photometric redshift bins from $z = 0.2$ to 1.2. The number density is 48 arcmin^{-2} . For the source galaxy samples, we assume the number density to be 27 arcmin^{-2} and split them into five redshift bins from $z = 0.2$ to 4. The cluster samples are generated using the richness–mass relation obtained in [7], and are split into four equally spaced redshift bins from $z = 0.2$ to 1. In the analysis, we assume a $w\text{CDM}$ cosmological model with w_0 and w_a describing the dark energy equation of state and its redshift dependence.

In figures 11 and 12, we compare the result of LINNA with the result obtained from the brute force method. We find that the level of agreement is consistent with what we found in analyzing DES

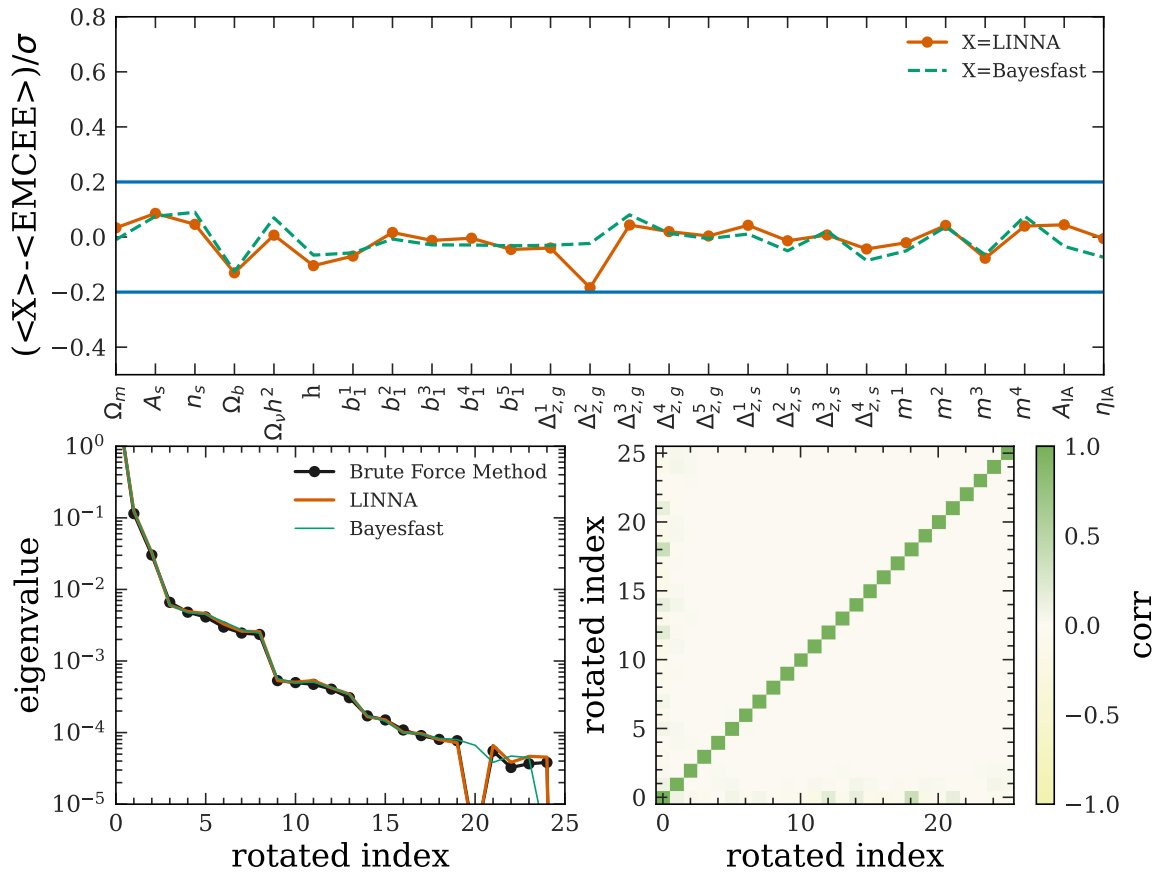


Figure 9. Similar to figure 7 but on the 3×2 pt data vector.

Y1 data. These results indicate that LINNA is expected to be applicable on the analysis of data with LSST Y10 precision.

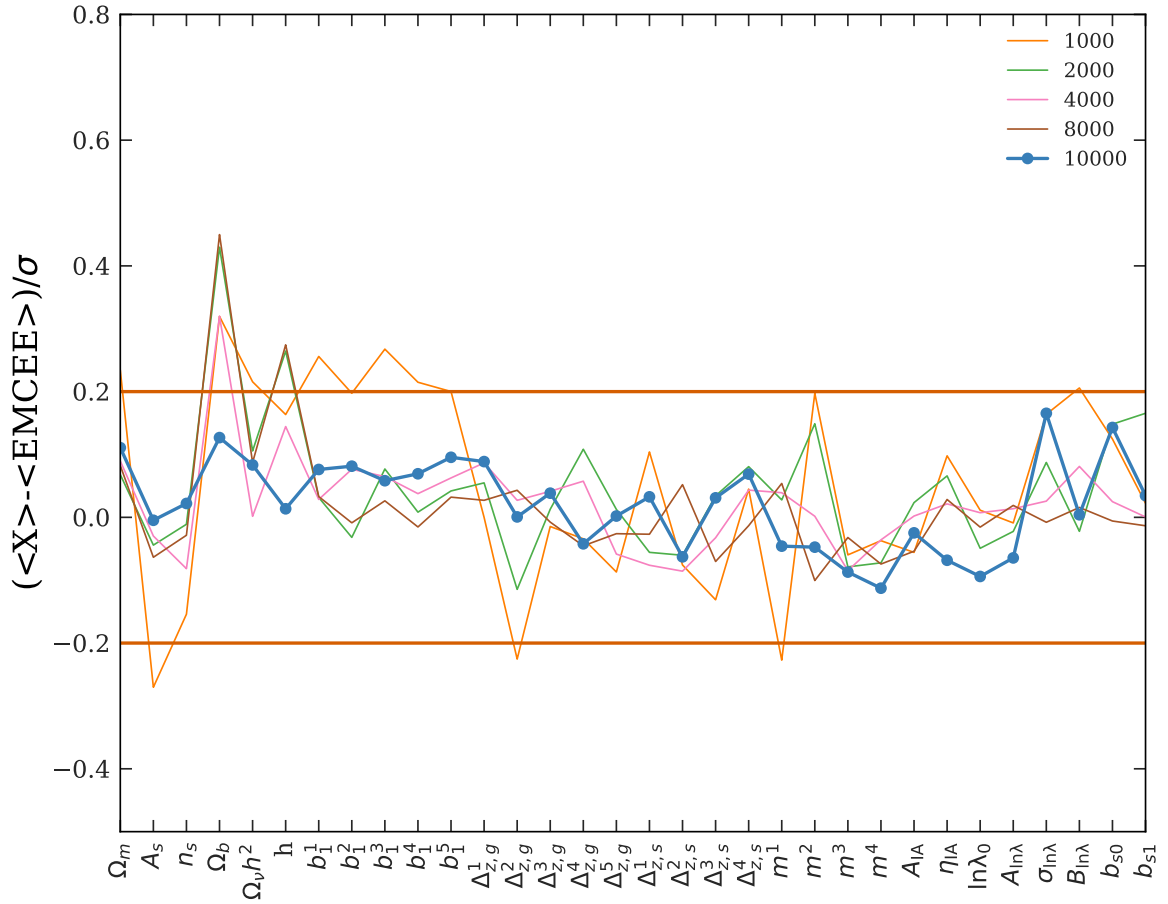


Figure 10. A comparison of LINNA performance with different numbers of training data points. The y axis shows the shifts in parameter mean estimations using LINNA and using the brute force method in the unit of 1σ uncertainties. Different color lines correspond to LINNA having 1000 – 10000 additional training data points per iteration.

Table 1. Breakdowns of LINNA run time in each component using the default option. Model shows the amount of time spent in generating the training data using CosmoLike. Train shows the time spent in training the neural network. MCMC shows the time spent in sampling the posterior using EMCEE. Numbers in each panel are in units of hours. Numbers in the parentheses show run time for LINNA with 2000 training data points in each iteration.

Analysis: $6 \times 2pt + N$

	iteration 1	iteration 2	iteration 3	iteration 4	Total
Model	1.12 (0.46)	0.67 (0.18)	0.74 (0.19)	0.78 (0.19)	3.31 (1.02)
Train	0.51 (0.56)	0.61 (0.61)	1.23 (0.56)	1.25 (0.69)	3.60 (2.42)
MCMC	0.29 (0.30)	0.28 (0.25)	0.51 (0.58)	2.08 (2.33)	3.16 (3.46)
Total	1.93 (1.32)	1.55 (1.05)	2.48 (1.33)	4.11 (3.21)	10.07 (6.89)

Analysis: $4 \times 2pt + N$

	iteration 1	iteration 2	iteration 3	iteration 4	Total
Model	1.05 (0.74)	0.69 (0.25)	0.71 (0.26)	0.72 (0.26)	3.18 (1.51)
Train	0.73 (0.22)	0.89 (0.38)	1.09 (0.52)	1.57 (0.52)	4.28 (1.64)
MCMC	0.26 (0.44)	0.30 (0.48)	0.61 (1.57)	2.82 (6.76)	3.99 (9.25)
Total	2.05 (1.40)	1.88 (1.11)	2.42 (2.35)	5.11 (7.54)	11.45 (12.40)

Analysis: $3 \times 2pt$

	iteration 1	iteration 2	iteration 3	iteration 4	Total
Model	0.55 (0.35)	0.14 (0.04)	0.14 (0.08)	0.14 (0.04)	0.99 (0.51)
Train	0.48 (0.26)	0.63 (0.62)	0.80 (0.33)	1.25 (0.46)	3.16 (1.67)
MCMC	0.20 (0.21)	0.21 (0.20)	0.29 (0.28)	0.56 (0.57)	1.25 (1.26)
Total	1.23 (0.82)	0.98 (0.86)	1.24 (0.70)	1.95 (1.06)	5.39 (3.44)

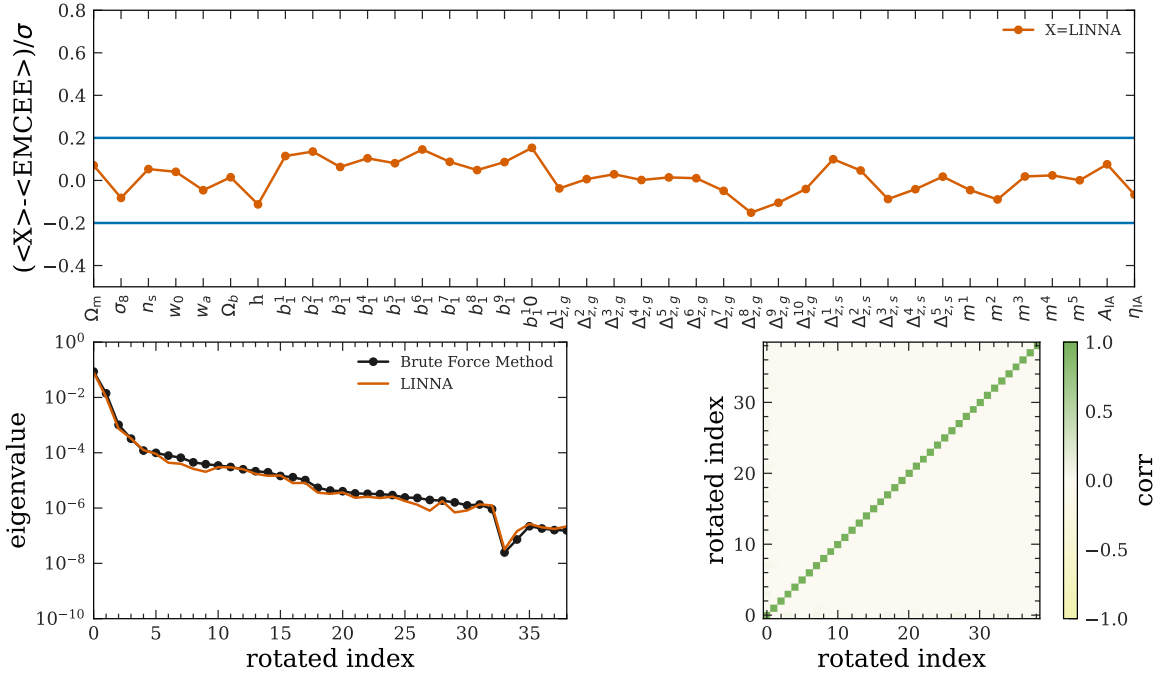


Figure 11. Performance of LINNA on the 3×2 pt analysis using the simulated LSST Y10 data vector. Details of this plot are similar to figure 7.

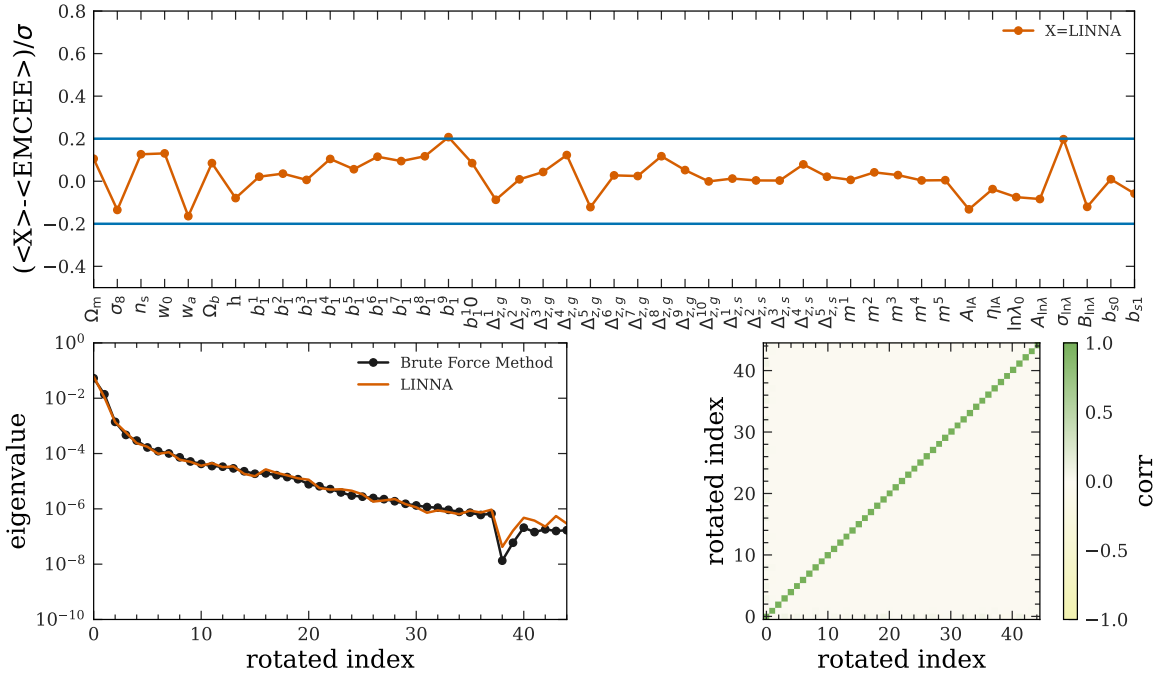


Figure 12. Performance of LINNA on the 6×2 pt+N analysis using the simulated LSST Y10 data vector. Details of this plot are similar to figure 7.